Depolymerization Characteristics during the Pyrolysis of Two Industrial Lignins

Jiangyong Chu, Weikun Jiang, and Shubin Wu*

For the value-added utilization of industrial lignin both from pulping black liquor and acid hydrolysis residues, the eucalyptus alkali lignin (AL) and enzymatic mild acidolysis corncob-to-xylitol residue lignin (EMARL) were isolated. Their pyrolysis behaviors were investigated by thermogravimetric analysis (TGA), *in situ* Fourier transform infrared spectroscopy (FTIR), and pyrolysis-gas chromatography/mass spectrometry (Py-GC/MS). The chemical bonds of EMARL were easier to break than AL at relatively lower temperatures, which was confirmed by the relationship between temperature and the differential absorbance of functional groups (such as carbonyl and hydroxyl). Based on the analysis of pyrolysis products, the value-added monomers were the main products. At 400 °C, AL mainly contained guaiacyl-type and syringyl-type compounds and the yields were 28.95% and 62.54%, respectively, while EMARL contained more guaiacyl-type products (62.96%). When the temperature was increased to 600 °C, the contents of phenol-type increased, suggesting that the demethoxylation reaction occurred during lignin pyrolysis. Study of the characteristics of pyrolysis could be significant for understanding the thermochemical depolymerization of AL and EMARL for value-added products.

Keywords: Industrial lignin; Pyrolysis; Py-GC/MS; In situ FTIR

*Contact information: State Key Lab of Pulp & Paper Engineering, South China University of Technology, Guangzhou, Guangdong 510640, China; *Corresponding author: shubinwu@scut.edu.cn*

INTRODUCTION

With the ever-increasing depletion of fossil fuels and deterioration of the environment, the exploitation of renewable resources for the production of fuels, chemicals, and energy has gained much attention. Efforts have been made to find green and sustainable resources for new energy sources and materials (Liu *et al.* 2015). Naturally abundant and renewable resources such as lignocellulosic biomass are potential replacements to fossil fuels (Norgren and Edlend 2014). Lignocellulosic biomass primarily consists of three polymeric components: cellulose (C6-sugars), hemicellulose (mainly C5-sugars), and lignin. The hemicellulose and cellulose fractions can be transformed into various types of biofuels, such as bio-ethanol, bio-butanol, and bio-gasoline (Alonso *et al*. 2010; Serrano-Ruiz *et al*. 2010). These transformations can occur *via* three major routes: biochemical, catalytic, and thermochemical (Huber *et al*. 2006; Anex *et al*. 2010; Kim *et al*. 2013). Present technologies can efficiently transform cellulose and hemicellulose into bio-based chemicals and fuels, but lignin is highly underutilized.

Compared with cellulose and hemicellulose, lignin is a complex three-dimensional amorphous polymer composed of three different cinnamyl alcohol monomers: *p*-coumaryl alcohol, coniferyl alcohol, and sinapyl alcohol (Upton and Kasko 2015).

Lignin is a heterogeneous aromatic biopolymer that accounts for nearly 30% of the organic carbon on earth, and it is also one of the few renewable aromatic sources (Zakzeski *et al*. 2010). If depolymerized efficiently, it can produce value-added chemicals and fuels. However, lignin in large quantities is produced as a waste in many industrial processes, such as pulp production and

the production of bioethanol from lignocelluloses. Over one million tons of lignin are produced per year as a byproduct of the paper and pulp industry, and this value is poised to increase from the emerging biomass refinery industry (Glasser *et al.* 1999). Only approximately 2% of the lignin available from the pulp and paper industry is used commercially, with the remainder being burned as a low-value fuel (Lou *et al.* 2010).

Because of its aromaticity, lignin is a potential feedstock for producing the value-added phenolic-rich bio-oil. Thus, the mechanism by which lignin is pyrolytically converted to products needs to be clarified for the advancement of biofuels and chemicals. The structure of lignin is more complex and unordered than those of cellulose and hemicelluloses, leading to a complex decomposition mechanism. The most significant challenge in using lignin for pyrolysis mechanism studies is the limited understanding of its thermal degradation behaviors. Many previous studies mainly pay close attention to the characterization of pyrolysis products (Lou *et al*. 2010; Lou and Wu 2011); therefore, characterization of the original lignin structure and its influence on pyrolysis behavior are inadequate.

The lignin pyrolysis mechanism is usually investigated using a thermogravimetric analyzer coupled with a Fourier transform infrared spectrometer (TG-FTIR) and a pyrolyzer equipped with gas chromatography/mass spectrometry (Py-GC/MS). The main pyrolysis products and the maximum weight loss rates are quite different for various wood species (Liu *et al.* 2008). TG-FTIR identifies the organic compounds with similar chemical functional groups but cannot separate single species from the FTIR spectra. Hence, the fast pyrolysis of enzymatic/mild acidolysis lignin has been studied by Py-GC/MS; the obtained pyrolysis products are composed of heterocycles, phenols, esters, and a small amount of acetic acid (Lou *et al.* 2010). Analysis of the pyrolysis behavior of different lignin polymers shows that thermally unstable ether bonds and side branches are well-preserved in alkali lignin and milled wood lignin but are broken in organosolv lignin and klason lignin (Wang *et al*. 2015). In mill wood lignin isolated from hardwood and softwood, the methoxy group content has a significant influence on the resulting pyrolysis behaviors (Wang *et al*. 2009). Klason lignin has been used as a model compound to compare the pyrolysis behaviors of hardwood and softwood lignins. Radical formation during hardwood klason lignin pyrolysis is more frequent than that of softwood klason lignin pyrolysis, and it is mainly affected by the amount of methoxy groups in the hardwood klason lignin (Bährle *et al.* 2014).

This study investigated the thermal degradation behaviors of two industrial lignins. For this purpose, the absorbance evolution of functional groups at various temperatures was analyzed by *in situ* FTIR, which was analysis of the not gaseous byproducts of pyrolysis, and the resulting products were measured by Py-GC/MS to determine their composition and yields. Conventional analysis methods of the peak area% are poor comparisons of the different lignin yields. Hence, a novel peak areas analysis method was used to quantify the pyrolytic products in this study.

EXPERIMENTAL

Materials

Alkali lignin (AL) was obtained from in-house eucalyptus sulfate pulping black liquor. The pulping method and chemical properties of the black liquor have been previously reported (Zhang and Liu 2012). The isolation and purification methods were also reported in a previous study (Sun *et al.* 2002). Corncob-to-xylitol residue lignin was isolated from corncob acid hydrolysis residue, which was adopted through the modified enzymatic mild acidolysis method (Lou and Wu 2011). The molecular formula of the two lignins was determined from the elemental analysis, giving $C_9H_{9.6901}O_{3.1665}N_{1.1064}S_{0.5621}$ for AL and $C_9H_{10.1284}O_{3.7497}N_{2.347}S_{0.0045}$ for EMARL (enzymatic mild acidolysis corncob-to-xylitol residue lignin).

Experimental Methods

Thermogravimetric analysis (TGA)

The thermal characteristics of two kinds of lignin were analyzed by thermal gravimetric analysis equipment (TA Q500, TA Instruments, New Castle, DE, USA). Approximately 5 mg to 10 mg of lignin was used for each test. The temperature was raised from room temperature to 700 °C at a heating rate of 20 °C/min. The measurements were carried out using high purity N_2 with a gas flow rate of 25 mL/min.

In situ diffuse reflectance infrared pyrolysis device

In situ Fourier transform infrared spectroscopy (FTIR) (Nicolet IS50, Thermo Fisher Scientific, Waltham, MA, USA) and an *in situ* pool with a deuterated sulfuric acid GSH detector were adopted in this experiment. To ensure full beam transmittance and good heat resistance, CaF_2 with protective water-cooling was used for the window. The real time temperature of the *in situ* pool was adjusted using a temperature controller with a proportion, integration, and differentiation (PID) thermo-coupling controller, and the accuracy of the temperature control was ± 1 °C. Specific operation parameters were as follows: nitrogen with a purity of 99.999% was used to purge the system at a rate of 1 L/min for 15 min to maintain an inert atmosphere, after which the intake and outlet valves were closed to ensure that the pyrolysis process was carried out under sealed conditions. The temperature was increased from room temperature to 670 °C at a rate of 40 °C/min and was held at 670 °C for 10 min. The spectral scanning range was 650 cm^{-1} to 4000 cm^{-1}, the resolution was 4 cm^{-1}, and the sampling interval was 1.93 s. A N_2 atmosphere at 100 °C was selected as the spectral background. *In situ* FTIR could detect the absorbance of functional groups in real-time. According to the heating rate, the relationship between absorbance and temperature was calculated, and the first derivative of absorbance with temperature was also be established.

Py-GC/MS analysis

Fast pyrolysis experiments for two kinds of lignin were conducted using the pyrolyzer (Tandem u-Reactor Rx-3050TR, Frontier Laboratories Ltd., Koriyama, Japan) with direct connection to a gas chromatography coupled with a mass spectrometer (GC/MS) (Agilent 7890B, Santa Clara, CA, USA). In each experiment, about 0.5 mg lignin (m_1) was placed in a quartz filler tube. The pyrolysis temperature was set from room temperature to the different terminal temperature at 400 °C, 500 °C, and 600 °C with a fixed heating rate of 20 °C/ms and a fixed residence time of 20 s. The pyrolysis volatiles were analyzed online by GC/MS, and the transfer line and injector temperature were kept at 300 °C. The chromatographic separation was performed using a TR-5MS capillary column (Agilent HP6890-5973 quartz capillary column, 30 mm × 0.25 mm × 0.25 mm). Helium (99.999%) was used as the carrier gas with a constant flow rate of 1

mL/min and a 50:1 split ratio. The oven temperature was programmed from 50 °C (2 min) to 90 °C (3 min) at a heating rate of 10 °C/min, then the temperature was programmed from 90 °C (3 min) to 150 °C (50 min) at the heating rate of 3 °C/min, and lastly the program was heated to 350 °C (3min) at the heating rate of 20 °C/min. The temperature of the GC/MS interface was held at 300 °C, and the mass spectrometer was operated in EI mode at 70 eV. The mass spectra were obtained from 20 m/z to 400 m/z with the scan rate of 500 $amus^{-1}$. The pyrolysis products were analyzed by the NIST library, and the peak areas of each detected product was abbreviated as P_a. The P_m was calculated by Eq. 1.

$$P_m = P_a/m_1 \quad (1)$$

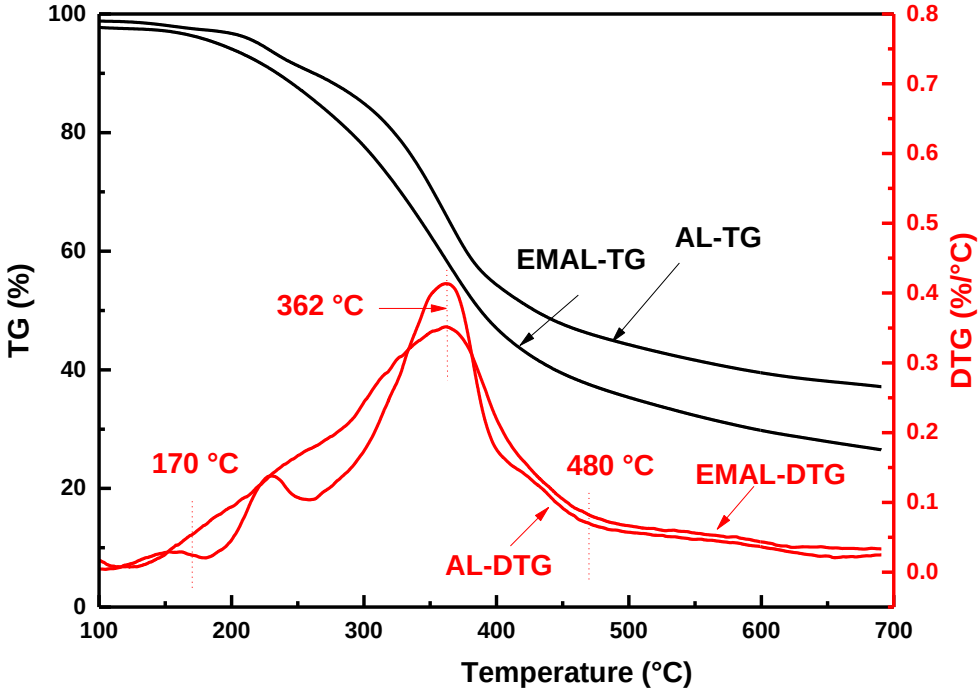

Fig. 1. Thermogravimetric curve (TG) and differential thermogravimetric curve (DTG) of AL and EMARL at 20 °C/min under N_2

RESULTS AND DISCUSSION

Thermal Weight-Loss Analysis

To determine the decomposition temperatures, devolatilization rates, and mass fractions of two lignin samples, thermogravimetric (TG) and first derivative thermogravimetric (DTG) curves during the thermal decomposition of AL and EMARL as functions of the temperature were calculated, as depicted in Fig. 1. Generally, the thermal degradation process could be divided into three distinct weight loss stages within a temperature range of 100 °C to 700 °C. The first stage was a loss in weight upon drying the sample (below 170 °C), mainly due to water released by evaporation and dehydration. The second stage was fast thermal decomposition between 170 °C and 480 °C. The main mass loss of the two lignins appeared at this range, as reported previously (Wang *et al.* 2014; Li *et al.* 2014), and corresponded to the release of phenylpropane units (Jakab *et al.* 1995). About 52 mass% and 60 mass% of AL and EMARL were converted into volatiles, respectively. This result suggested that more EMARL could convert into volatiles than AL. In

addition, the maximum rate of degradation from AL and EMARL was at approximately 362 °C, and the maximum devolatilization rate (0.43%/°C) of AL was slightly higher than that of EMARL (0.36 %/°C). The weight loss was 10 mass% less in the final stage (after 480 °C), and it mainly involved the formation of char residues instead of bio-oil (Wang *et al.* 2014a). AL left more residues (about 38 mass %) than EMARL (about 28 mass %) at around 700 °C. The solid residue indicated condensation and polymerization reactions during the heating process. This result was also confirmed by the following Py-GC/MS experiments.

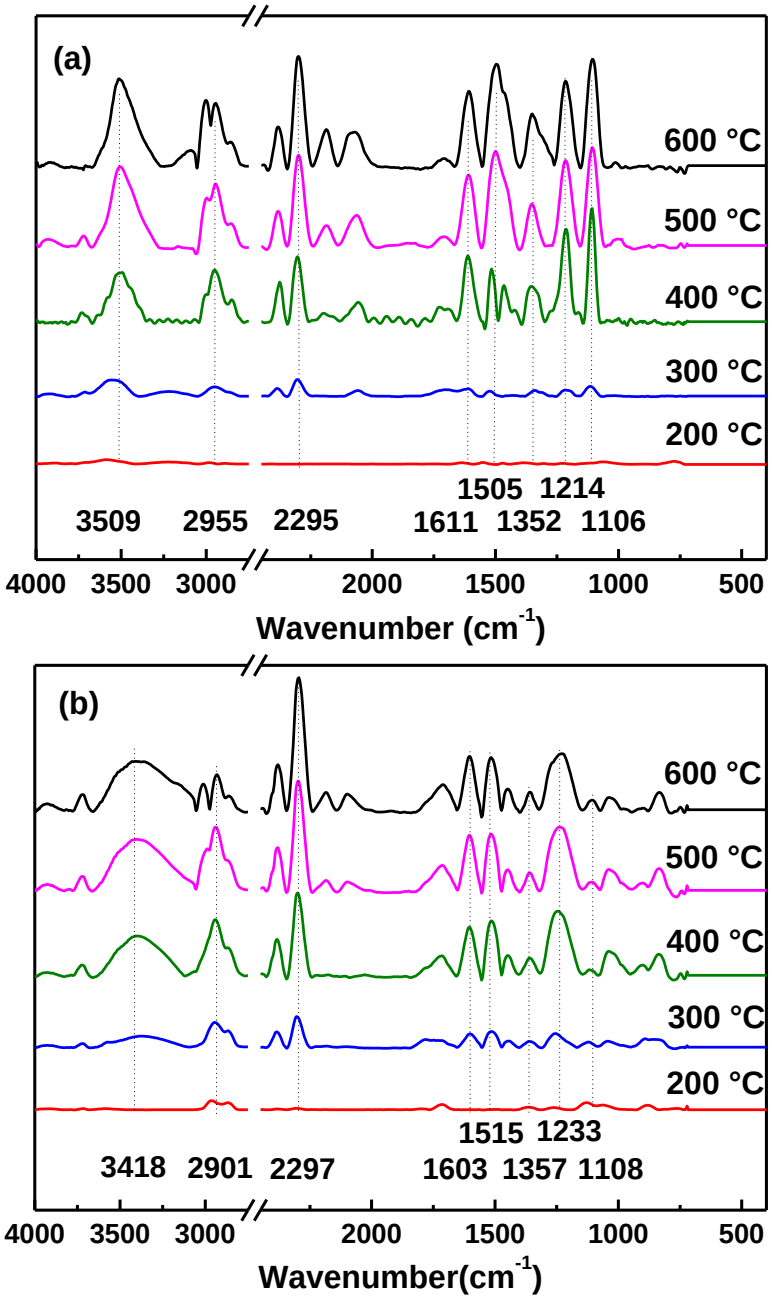

Fig. 2. The temperature-dependent infrared spectral distributions of AL (a) and EMAL (b)

In situ FTIR Analysis

The small volatile molecules that were produced during the pyrolysis of lignin with changing temperature were analyzed by *in situ* FTIR, and the pyrolytic results are displayed in Fig. 2. The *in situ* FTIR analysis was carried out on evolved volatile components. The absorbance peaks agreed well with the weight-loss in the derivative thermogravimetry (DTG) curve (shown in Fig. 1), where the degradation in the second stage mainly occurred between 300 °C and 400 °C. The peaks at 3509 cm^{-1} and 3418 cm^{-1} (shown in Fig. 2(a) and (b), respectively) were due to the stretching vibration of hydroxyl group. The absorbance at 2955 cm^{-1} and 2901 cm^{-1} corresponded to C-H linkages. The bands at 1611 cm^{-1} and 1605 cm^{-1} corresponded to conjugated C=O groups. The absorbance seen at 1505 cm^{-1} and 1515 cm^{-1} belonged to the aromatic skeleton. The stretching vibration of C-O linkage appeared within the range of 1200 cm^{-1} to 1360 cm^{-1}. The intensities of the bands at 1106 cm^{-1} and 1108 cm^{-1} were associated with the syringyl structure of the lignin (Jahan *et al.* 2014). In addition, some non-condensable gaseous components with low molecular weights were easily identified by their prominent characteristic peaks such as CO (at around 2010 cm^{-1}), CO_2 (at around 2300 cm^{-1}), CH_4 (at around 3000 cm^{-1}), and H_2O (at around 3700 cm^{-1}).

The relationship between the absorption intensity of functional groups and temperature is shown in Fig. 3. As shown in Fig. 3 (a, c), the hydroxyl functional groups (3526 cm^{-1}, 3418 cm^{-1}) from two lignin samples were first observed at 250 °C, and the absorbance rapidly increased with the temperature increasing to 450 °C. With further increases in temperature, the absorbance remained mostly steady. The peak of C-H (3013 cm^{-1}, 3016 cm^{-1}) corresponding to the emission of CH_4 (Wang *et al.* 2009; Chen *et al.* 2015), appeared at about 350 °C. With the temperature rising, the absorbance also rapidly increased after 350 °C. Notably, the temperature that the absorbance of C-H began to rise, 350 °C, was higher than other functional groups. This result suggested that large quantities of monomer phenols with active functional groups were formed by the cleavage of ether linkages (Brebu *et al.* 2013). After that, these chemical linkages (-OCH_3, -OH, C=O, *etc.*) further fell off to form monomers of low molecular weights.

The intensity of the CO_2 absorption peak (2295 cm^{-1}, 2297 cm^{-1}) grew rapidly between 250 °C and 450 °C, and then continued to gradually increase with the temperature rising, indicating that CO_2 was mainly generated between 250 °C and 450 °C during the pyrolysis progress. The formation of CO_2 derived from carboxyl meant that decarboxylation reaction had occurred in the whole pyrolysis process but mainly happened between 250 °C and 450 °C.

The carbonyl group on the side chains caused a conjugated effect with the benzene ring, resulting in the detection of conjugated C=O groups (1611 cm^{-1} in AL and 1603 cm^{-1} in EMARL). The C-C stretching vibrations in the aromatic skeleton are shown in Fig. 3b (1514 cm^{-1}) and Fig. 3d (1515 cm^{-1}) (Tejado *et al.* 2007). They showed no obvious changes before 200 °C, but rapidly increased between 200 °C and 450 °C. This result indicated that aromatic volatile compounds emerged during this temperature region. After 500 °C, the absorbance of C-C linkage dropped slightly, possibly due to the cleavage of parts of the aromatic rings.

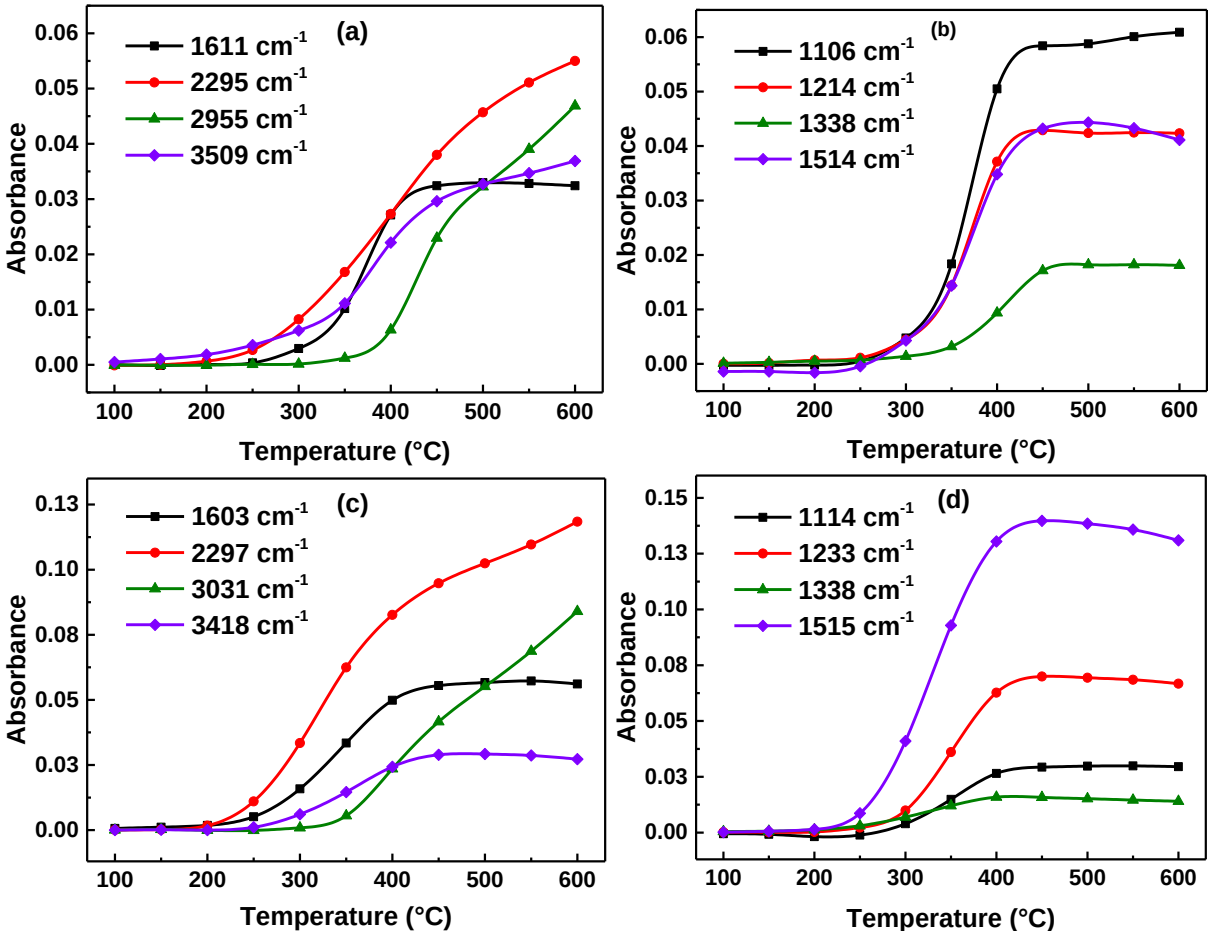

Fig. 3. Variation in absorption intensity with temperature for AL and EMARL: (a) IR peak intensities of AL in the region 4000 cm^{-1} to 1600 cm^{-1}; (b) IR peak intensities of AL in the region 1600 cm^{-1} to 500 cm^{-1}; (c) IR peak intensities of EMARL in the region 4000 cm^{-1} to 1600 cm^{-1}; (d) IR peak intensities of EMARL in the region 1600 cm^{-1} to 500 cm^{-1}

In Fig. 3b, the absorbance of aromatic ethers (1214 cm^{-1}) gradually increased with temperature and then kept steady after 450 °C. Similar trends with C-C (1514 cm^{-1} in Fig. 3b) linkage were noticed. This result indicated that some functional groups were contained in the aromatic ring, such as methoxyl, which led to the production of the aromatic skeleton and C-O-C ether linkages simultaneously. As shown in Fig. 3d (1233 cm^{-1}), there was an obvious difference between the aromatic skeleton and ether linkage, which may be ascribed to the lower content of syringyl units in EMARL. CO originated from the rupture of ether bridges at a low temperature, while at a high temperature the dissociation of diaryl ether was the main source of CO production (Zhang *et al.* 2012). For AL (1106 cm^{-1} in Fig. 3b) and EMARL (1114 cm^{-1} in Fig. 3d), the concentration of hydrocarbons gradually increased with the temperature increasing and then kept steady after 450 °C. This mainly originated from the in-plane deformation vibration of the aromatic C-H linkage in the syringyl structure of lignin (Tejado *et al.* 2007). The dramatic difference between AL and EMARL is shown in Fig. 3b and Fig. 4d.

In contrast to the two kinds of lignin, one noticeable difference between AL and EMARL was that the temperature at which the greatest absorbance increase occurred was much lower in EMARL than AL. Another remarkable difference was that the maximum absorbance of all functional groups in EMARL emerged earlier than AL. In order to accurately confirm these

findings, the first derivative of absorbance was introduced in Fig. 4. Since the first derivative of the absorbance represented the variation rate of absorbance, the above phenomena could be confirmed by the turning points in Fig. 4. Other similar figures are shown in supplementary Fig. S1. Moreover, another significant result found was that the temperature corresponding to the maximum growth rate of the absorbance in EMARL was much lower than that of AL. These results could be explained by the structure of EMARL.

Compared to AL, the thermal unstable ether bonds and side branches were more well-preserved in EMARL, which led to the decomposition reaction occurring at a low temperature. However, the simultaneous evolution of several volatile compounds having similar chemical structures did not allow the identification of the single species by the analysis of the *in situ* FTIR spectra. Detailed information about the organic compounds formed during AL and EMARL pyrolysis were thus obtained from the Py–GC/MS instrument, and are discussed in the following section.

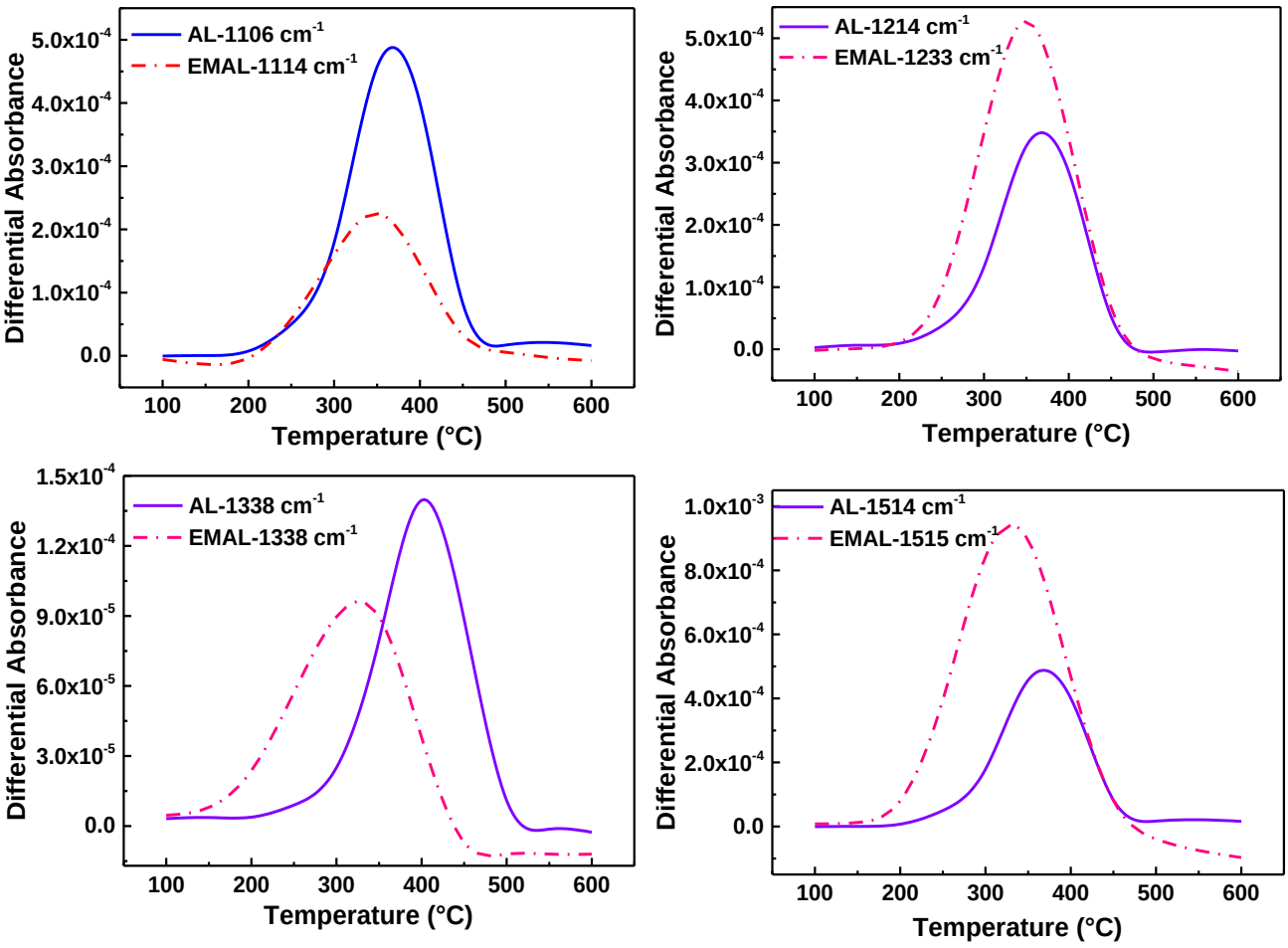

Fig. 4. Variation in differential absorbance with temperature for AL and EMARL. AL-1160cm^{-1} represented the differential absorbance of AL in 1160 cm^{-1}, EMAL-1114cm^{-1} represented the differential absorbance of EMAL in 1114 cm^{-1}, and so on.

Analysis of Aromatic Monomers

The components corresponding to each signal peak were identified based on the total ion chromatograms; the compounds and relative percentage of the released lignin pyrolysis products are shown in Table S1. It was not surprising that the products detected by GC/MS were mainly phenols. Most of these phenols were valuable pharmaceutical intermediates. As shown in Table S1, guaiacol, syringol, 4-methyl-syringol, and catechol were the main products in AL, while 4-vinyl-phenol, 4-methyl-guaiacol, 4-ethyl-guaiacol, 4-vinyl-guaiacol were the major products in EMARL. According to the Table S1, the results of pyrolysis products were extremely complex. However, based on the product structure, monomers were mainly classified into five types: (1) Phenol (P)-type, phenol, 4-methyl phenol, and 4-propenyl phenol et al. (2) Guaiacyl (G)-type, guaiacol, 2-methyl-guaiacol, and vanillin et al. (3) Syringyl (S)-type, syringol, 4-methyl-syringol, 4-hydroxy-3, 5-dimethoxy benzaldehyde et al. (4) Catechol (C)-type, catechol, 3-methoxyl-catechol et al. (5) Others (O)-type.

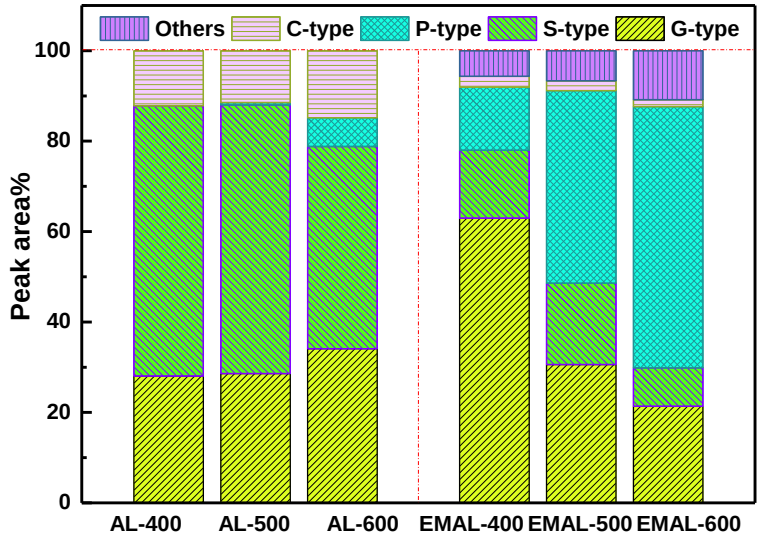

Fig. 5. The peak area% of different type products in various temperatures. AL-400 represents the pyrolysis of AL in 400 °C, EMARL-400 represents the pyrolysis of EMARL in 400 °C, and so on.

As shown in Table S1, the relative contents of each phenolic compound changed significantly with pyrolytic temperature. However, it was also interesting to consider the overall yield of G, S, P, C, and O type's compounds. Hence, the total peak area% of different type products in various temperatures can be seen in Fig. 5. The results demonstrated that G-type compounds and S-type compounds were the dominant products for AL, while the sum of P-type compounds and C-type compounds were notably increased with the elevated temperature. This result might be a consequence of the secondary cracking of the primary products with the temperature increasing, which resulted in the production of compounds with less side chains (Shen *et al*. 2010; Dong *et al*. 2012). The P-type compounds of EMARL were much higher than that of AL, and the yields were 13.92%, 42.61%, and 57.76% at 400 °C, 500 °C, and 600 °C, respectively. The P-type monomers mainly derived from G-type (The G-type products could be converted by S-type monomers) through the cleavage of Ar-OCH_3. In contrast, the S-type compounds produced from AL (59.77%, 59.43%, and 44.74%) were higher than that of

EMARL (15.04%, 17.98%, and 8.53%), which was consistent with previous research showing that AL contained more syringyl units (Wang *et al.* 2014b). The *in situ* FTIR analysis of AL and EMARL also supported this phenomenon, where the intensity of syringyl units in AL was much higher than others. The production of G-type compounds from EMARL decreased from 62.96% (400 °C) to 21.35% (600 °C), while P-type compounds increased from 13.92% to 57.76%. At lower pyrolysis temperature (400 ◦C), the depolymerization was not sufficient. Therefore large number of methoxyl (-OCH3) still linked on the phenylpropane unit. Then, as the temperature increasing, more and more methoxyl fell off from the phenylpropane units and transferred into CH_4. Thus, the P-type phenols increased with the depolymerization of S-type and G-type phenols. The C-type products of AL gradually increased with temperature, while the opposite result was observed in EMARL. The C-type compounds of EMARL were much lower than that of AL (12.18%, 11.47% and 14.79%, respectively), and the yields were 2.41%, 2.18%, and 1.54% at 400 °C, 500 °C, and 600 °C, respectively. The C-type monomers mainly derived from G-type (The G-type products could be converted by S-type monomers) through the cleavage of ArO-CH_3 to generate CH_4, which was different with the cleavage of Ar-OCH_3. The results indicated that the cleavage of Ar-OCH_3 linkage occurred more easily than the cleavage of ArO-CH_3 in EMARL. Furthermore, other products were formed in EMARL, such as toluene and butyraldehyde, but were nonexistent in AL. This result indicated that the thermally unstable ether bonds and side branches were well-preserved in EMARL, which caused the diversity of the pyrolysis products.

The semi-quantitative analysis results of the major products in AL and EMARL are shown in Fig. 6 (a) and (b), respectively. As shown in Fig. 6 (a), the amount of the 4-methyl-syringol and guaiacol increased and then decreased with the temperature increasing. The maximum amounts of 4-methyl-syringol (4.58×10^8), 4-propyl-syringol (1.25×10^8), and guaiacol (1.98×10^8) were obtained at 500 °C. With the temperature increasing, catechol and syringol showed different variation trends. The maximum yields of syringol and catechol (6.93×10^8, 2.47×10^8) were obtained at 400 °C and 600 °C, respectively. With an increase from 400 °C to 600 °C, the P_m of syringol quickly decreased from 6.93×10^8 to 2.67×10^8, while catechol continually increased from 2.24×10^8 to 2.47×10^8 with the temperature increase. Guaiacol is a precursor that decomposes to form catechol (Asmadi *et al.* 2011). The secondary cracking reactions (especially the demethoxylation reaction) of these pyrolysis products were promoted under higher temperatures.

As shown in Fig. 6 (b), the content of the 4-vinyl-phenol increased with the temperature increasing, especially between 400 °C and 500 °C. When the temperature increased from 400 °C to 600 °C, the P_m of 4-vinyl-phenol increased from 5.63×10^7 to 1.36×10^9, however, the P_m of 4-methy-guaiacol and 4-ethyl-guaiacol decreased from 1.48×10^9 to 7.46×10^7 and 6.17×10^8 to 4.28×10^7, respectively. These dramatic changes were attributed to the demethoxylation reaction for guaiacyl units, which was enhanced at higher temperatures (Asmadi *et al*. 2011). This was consistent with the analysis of the *in situ* FTIR and peak area% in different products. In AL, the main difference of the pyrolysis products happened between 500 °C and 600 °C, but the temperature region was 400 °C to 500 °C in EMARL. The linkages contained in the main chains of EMARL were more easily broken than those of AL at relatively low temperatures. The similar result is shown in Fig. 5. This was also consistent with *in situ* FTIR analysis that the maximum absorbance of functional groups in EMARL appeared at lower temperatures.

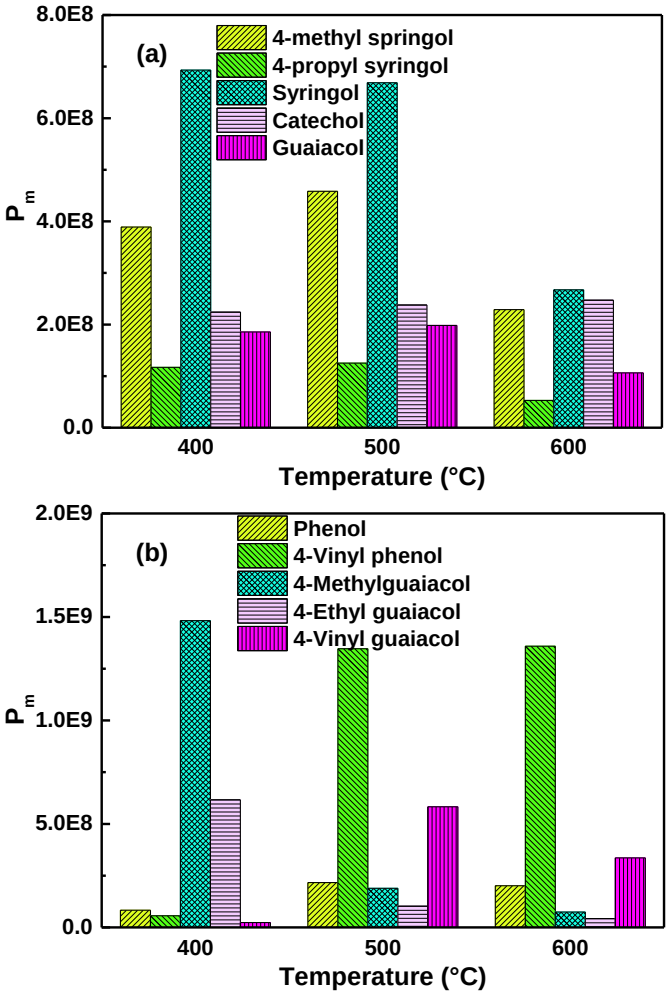

Fig. 6. Main compounds distributions of AL (a) and EMARL (b) pyrolysis in the Py-GC/MS analysis at different temperatures

CONCLUSIONS

1. Eucalyptus alkali lignin (AL) and enzymatic mild acidolysis corncob-to-xylitol residue lignin (EMARL) exhibited similar thermal behavior in terms of TG/DTG analysis, as almost identical maximum weight-loss temperatures were observed at around 362 °C. However, the decomposition of EMARL started at lower temperatures and the yield of char in EMARL was 26.5%, which was much lower than the yield of 37.1% in AL.
2. *In situ* FTIR analysis of evolved gaseous breakdown products indicated that the IR peak intensities of lignin sharply increased with the elevation of the pyrolysis temperatures, especially between 300 °C and 400 °C. Compared with AL, the absorbance of functional groups (such as C=O, O-H, C=C, *etc.*) in EMARL began to increase at a lower temperature and the maximum absorbance emerged earlier than AL. Moreover, the temperature which related to the maximum growth rate of the absorbance in EMARL was much lower than that of AL. Combined with the

absorbance and the first derivative of absorbance analysis, it could be confirmed that the depolymerization reaction of EMARL was much easier than that of AL.

3. For Py-GC/MS analysis, the main variation of the pyrolysis products occurred between 500 °C and 600 °C in AL, and between 400 °C and 500 °C in EMARL. G-type (AL 28.95%) and S-type (AL 62.54%) compounds were the predominant products at 400 °C in AL, while G-type (62.96%) was the main product in EMARL. As the temperature increased from 400 °C to 600 °C, the contents of P-type increased from 0% to 6.38% and 13.92% to 57.76%, respectively. The analysis of the P_m combined with the peak area% in different type products confirmed that methoxyl groups were released from the aromatic rings.

ACKNOWLEDGMENTS

The authors gratefully acknowledge the support of the Natural Sciences Foundation of China (No.31670582) and the National Basic Research Program of China (973 program, No. 2013CB228101).

REFERENCES CITED

Alonso, D. M., Bond, J. Q., and Dumesic, J. A. (2010). "Catalytic conversion of biomass to biofuels," *Green Chemistry* 12(9), 1493-1513. DOI: 10.1039/C004654J

Anex, R. P., Aden, A., Kazi, F. K., Fortman, J., Swanson, R. M., Wright, M. M., Satrio, J. A., Brown, R. C., Daugaard, D. E., Platon, A., Kothandaraman, G., *et al*. (2010). "Techno-economic comparison of biomass-to-transportation fuels via pyrolysis, gasification, and biochemical pathways," *Fuel* 89, 29-35. DOI: 10.1016/j.fuel.2010.07.015

Asmadi, M., Kawamoto, H., and Saka, S. (2011). "Thermal reactions of guaiacol and syringol as lignin model aromatic nuclei," *Journal of Analytical and Applied Pyrolysis* 92(1), 88-98. DOI: 10.1016/j.jaap.2011.04.011

Bährle, C., Custodis, V., Jeschke, G., van Bokhoven, J. A., and Vogel, F. (2014). "*In situ* observation of radicals and molecular products during lignin pyrolysis," *ChemSusChem* 7(7), 2022-2029. DOI: 10.1002/cssc.201400079

Brebu, M., Tamminen, T., and Spiridon, I. (2013). "Thermal degradation of various lignins by TG-MS/FTIR and Py-GC-MS," *Journal of Analytical and Applied Pyrolysis* 104, 531-539. DOI: 10.1016/j.jaap.2013.05.016

Chen, L., Wang, X., Yang, H., Lu, Q., Li, D., Yang, Q., and Chen, H. (2015). "Study on pyrolysis behaviors of non-woody lignins with TG-FTIR and Py-GC/MS," *Journal of Analytical and Applied Pyrolysis* 113, 499-507. DOI: 10.1016/j.jaap.2015.03.018

Dong, C. Q., Zhang, Z. F., Lu, Q., and Yang, Y. P. (2012). "Characteristics and mechanism study of analytical fast pyrolysis of poplar wood," *Energy Conversion and Management* 57, 49-59. DOI: 10.1016/j.enconman.2011.12.012

Glasser, W. G., Northey, R. A., and Schultz, T. P. (eds.). (1999). *Lignin: Historical, Biological, and Materials Perspectives*, American Chemical Society, Washington, D.C.

Huber, G. W., Iborra, S., and Corma, A. (2006). "Synthesis of transportation fuels from biomass: Chemistry, catalysts, and engineering," *Chemical Reviews* 106(9), 4044-4098. DOI: 10.1021/cr068360d

Jahan, M. S., Chowdhury, D. N., Islam, M. K., and Moeiz, S. I. (2007). "Characterization of lignin isolated from some nonwood available in Bangladesh," *Bioresource Technology* 98(2), 465-469. DOI: 10.1016/j.biortech.2006.01.005

Jakab, E., Faix, O., Till, F., and Székely, T. (1995). "Thermogravimetry/mass spectrometry study of six lignins within the scope of an international round robin test," *Journal of Analytical and Applied Pyrolysis* 35(2), 167-179. DOI: 10.1016/0165-2370(95)00907-7

Kim, J., Sen, S. M., and Maravelias, C. T. (2013). "An optimization-based assessment framework for biomass-to-fuel conversion strategies," *Energy & Environmental Science* 6(4), 1093-1104. DOI: 10.1039/C3EE24243A

Liu, Q., Wang, S., Zheng, Y., Luo, Z., and Cen, K. (2008). "Mechanism study of wood lignin pyrolysis by using TG–FTIR analysis," *Journal of Analytical and Applied Pyrolysis* 82(1), 170-177. DOI: 10.1016/j.jaap.2008.03.007

Liu, W. J., Jiang, H., and Yu, H. Q. (2015). "Thermochemical conversion of lignin to functional materials: A review and future directions," *Green Chemistry* 17(11), 4888-4907. DOI: 10.1039/C5GC01054C

Lou, R., Wu, S. B., and Lv, G. J. (2010). "Fast pyrolysis of enzymatic/mild acidolysis lignin from moso bamboo," *BioResources* 5(2), 827-837. DOI: 10.15376/biores.5.2.827-837

Lou, R., and Wu, S. B. (2011). "Products properties from fast pyrolysis of enzymatic/mild acidolysis lignin," *Applied Energy* 88(1), 316-322. DOI: 10.1016/j.apenergy.2010.06.028

Li, B., Lv, W., Zhang, Q., Wang, T., and Ma, L. (2014). "Pyrolysis and catalytic pyrolysis of industrial lignins by TG-FTIR: Kinetics and products," *Journal of Analytical and Applied Pyrolysis* 108, 295-300. DOI: 10.1016/j.jaap.2014.04.002

Norgren, M., and Edlund, H. (2014). "Lignin: Recent advances and emerging applications," *Current Opinion in Colloid & Interface Science*, 19(5), 409-416. DOI: 10.1016/j.cocis.2014.08.004

Sun, R., Sun, X. F., Wang, S. Q., Zhu, W., and Wang, X. Y. (2002). "Ester and ether linkages between hydroxycinnamic acids and lignins from wheat, rice, rye, and barley straws, maize stems, and fast-growing poplar wood," *Industrial Crops and Products*, 15(3), 179-188. DOI: 10.1016/S0926-6690(01)00112-1

Serrano-Ruiz, J. C., West, R. M., and Dumesic, J. A. (2010). "Catalytic conversion of renewable biomass resources to fuels and chemicals," *Annual Review of Chemical and Biomolecular Engineering* 1, 79-100. DOI: 10.1146/annurev-chembioeng-073009-100935

Shen, D. K., Gu, S., Luo, K. H., Wang, S. R., and Fang, M. X. (2010). "The pyrolytic degradation of wood-derived lignin from pulping process," *Bioresource Technology* 101(15), 6136-6146. DOI: 10.1016/j.biortech.2010.02.078

Tejado, A., Pena, C., Labidi, J., Echeverria, J. M., and Mondragon, I. (2007). "Physico-chemical characterization of lignins from different sources for use in phenol–formaldehyde resin synthesis," *Bioresource Technology* 98(8), 1655-1663. DOI: 10.1016/j.biortech.2006.05.042

Upton, B. M., and Kasko, A. M. (2015). "Strategies for the conversion of lignin to high-value polymeric materials: Review and perspective," *Chemical Reviews* 116(4), 2275-2306. DOI: 10.1021/acs.chemrev.5b00345

Wang, S., Wang, K., Liu, Q., Gu, Y., Luo, Z., Cen, K., and Fransson, T. (2009). "Comparison of the pyrolysis behavior of lignins from different tree species," *Biotechnology Advances* 27(5), 562-567. DOI: 10.1016/j.biotechadv.2009.04.010

Wang, C., Lyu, G., Yang, G., Chen, J., and Jiang, W. (2014a). "Characterization and hydrothermal conversion of lignin produced from corncob acid hydrolysis residue," *BioResources* 9(3), 4596-4607. DOI: 10.1007/s12155-012-9266-3

Wang, S., Lin, H., Ru, B., Sun, W., Wang, Y., and Luo, Z. (2014b). "Comparison of the pyrolysis behavior of pyrolytic lignin and milled wood lignin by using TG–FTIR analysis," *Journal of Analytical and Applied Pyrolysis* 108, 78-85. DOI: 10.1016/j.jaap.2014.05.014

Wang, S., Ru, B., Lin, H., Sun, W., and Luo, Z. (2015). "Pyrolysis behaviors of four lignin polymers isolated from the same pine wood," *Bioresource Technology* 182, 120-127. DOI: 10.1016/j.biortech.2015.01.127

Zakzeski, J., Bruijnincx, P. C., Jongerius, A. L., and Weckhuysen, B. M. (2010). "The catalytic valorization of lignin for the production of renewable chemicals," *Chemical Reviews* 110(6), 3552-3599. DOI: 10.1021/cr900354u

Zhang, C. J., and Liu, Y. (2012). "Componential analysis of black liquor and determining of dissolution lignin," *Paper and Papermaking* 31(1), 63-64.

Zhang, M., Resende, F. L., Moutsoglou, A., and Raynie, D. E. (2012). "Pyrolysis of lignin extracted from prairie cordgrass, aspen, and kraft lignin by Py-GC/MS and TGA/FTIR," *Journal of Analytical and Applied Pyrolysis* 98, 65-71. DOI: 10.1016/j.jaap.2012.05.009

Article submitted: May 15, 2017; Peer review completed: July 22, 2017; Revised version received and accepted: August 10, 2017; Published: August 21, 2017.
DOI: 10.15376/biores.12.4.7241-7254